NASA Technical Memorandum 109175

Design and Evaluation of a Foam-Filled Hat-Stiffened Panel Concept for Aircraft Primary Structural Applications

D. R. Ambur
Langley Research Center, Hampton, Virginia

January 1995

National Aeronautics and
Space Administration
Langley Research Center
Hampton, Virginia 23681-0001

Design And Evaluation Of A Foam-Filled Hat-Stiffened Panel Concept For Aircraft Primary Structural Applications

Damodar R. Ambur
NASA Langley Research Center
Hampton, VA 23681-0001

Abstract

A structurally efficient hat-stiffened panel concept that utilizes a structural foam as stiffener core has been designed for aircraft primary structural applications. This stiffener concept utilizes a manufacturing process that can be adapted readily to grid-stiffened structural configurations which possess inherent damage tolerance characteristics due to their multiplicity of load paths. The foam-filled hat-stiffener concept in a prismatically stiffened panel configuration is more efficient than most other stiffened panel configurations in a load range that is typical for both fuselage and wing structures. The prismatically stiffened panel concept investigated here has been designed using AS4/3502 preimpregnated tape and Rohacell foam core and evaluated for its buckling and postbuckling behavior with and without low-speed impact damage. The results from single-stiffener and multi-stiffener specimens suggest that this structural concept responds to loading as anticipated and has good damage tolerance characteristics.

Introduction

Geodesically-stiffened structures are very efficient for carrying combined bending, torsion, and pressure loads that are typical of aircraft primary structures. They are also very damage tolerant since there are multiple load paths available to redistribute loads compared to prismatically stiffened structures (Refs. 1-2). Geodesically stiffened structures utilize continuous filament composite materials which make these structures amenable to automated manufacturing processes that reduce cost. The current design practice for geodesically stiffened structures is to use a solid-blade construction for the stiffener. This stiffener configuration is not an efficient concept and there is a need to identify other stiffener configurations that are more efficient but utilize the same manufacturing process as the solid blade.

The present paper describes a foam-filled stiffener cross-section that is more efficient than a solid-blade stiffener in the load range corresponding to primary structures. A prismatic hat-stiffener panel design is then selected for structural evaluation in uni-axial compression with and without impact damage. Experimental results for both single-stiffener and multi-stiffener panel specimens with and without low-speed impact damage are presented. Finite element analysis results are presented that predict the buckling and postbuckling response of the test specimens. Analytical results for both the element and panel specimens are compared with experimental results.

Foam-filled Stiffener Concepts

In order to make the solid-blade stiffener shown in Figure 1 more efficient, it is necessary to position the 0° material away from the skin to increase bending stiffness. When such a stiffener concept is applied to a geodesically stiffened structural configuration, the tooling design becomes extremely complicated since the tooling must be removed after curing. It is cost effective to leave the tooling inside the stiffener if the material for the tool is light in weight and has the necessary characteristics to withstand the processing environment during cure. If the material that is left in the stiffener has adequate mechanical properties, it could serve an additional purpose of supporting the stiffener webs and skin elements when the structure is loaded. In a typical manufacturing process, the overwrap material shown in Figure 1 is first placed in a female tool and unidirectional material is tow placed to form a predominantly 0° material stiffener cap. A pre-machined foam insert is then placed in the tool to complete the assembly which is then cured to produce the required geodesically stiffened structure. This fabrication procedure has the potential to produce grid-stiffened structures that have varied or tailored stiffnesses in different directions. As a first step toward evaluating this foam-filled stiffener concept for geodesically stiffened structures, it is necessary to study a much simpler prismatic stiffener concept to establish this concept.

Comparison of Structural Efficiencies

A design study was performed to compare the structural efficiency of the foam-filled structural concepts with the simpler, efficient, and more widely used hat-stiffener concept. The results presented in Figure 2 correspond to a 30-inch-long and 24-inch-wide panel with four stiffeners across the width. All panels are simply supported along the edges. The unidirectional tape material used in this study is the Hercules, Inc. AS4/3502 graphite-epoxy system with Rohacell WF-71 foam as the core material. This four-stiffener configuration is structurally the most efficient for load cases above 6000 lb/in. and has also been adapted for lower load cases in this study. A constrained optimization for minimum weight was performed using the Panel Analysis and Sizing COde (PASCO) from Reference 3 and the results for a range of axial loads from 3,000 to 20,000 lb/in. are presented in the figure. The results are presented as structural efficiency curves where the weight index W/AL of the panels are plotted against the load index N_x/L, where W is the panel weight, L is the length, A is the panel surface area, and N_x is the stress resultant in the x-direction. Results for solid-blade stiffened panel are also presented in this figure for comparison. The identification of commercial products in the present paper is intended to describe adequately the test specimens and does not constitute endorsement, expressed or implied, by the National Aeronautics and Space Administration.

These results indicate that the foam-filled hat-stiffened panel is lighter than the conventional hat-stiffened panel by approximately 6.5 percent for 6,000 lb/in. of applied load and approximately 10 percent for 20,000 lb/in. of applied load. The foam-filled blade-stiffened panel appears to perform better than the hat-stiffened panel above 16,000 lb/in. of applied load. The foam-filled hat-stiffened panel is lighter by about 20 percent when compared to the solid-blade concept. Hence, if the foam-filled hat-stiffened concept is used in stiffened structures, a substantial weight savings is possible over the entire load range considered (Ref. 2). A foam-filled hat-stiffened panel design for 3,000 lb/in. of applied load, which corresponds to a fuselage structure, has been chosen for evaluation in this paper.

The optimized design for this load case has a $(\pm 45/-45/\pm 45/-45/0)_S$ skin layup, $(\pm 45/0_5/-45/0_5/45/0_5/90)_S$ stiffener cap layup, and $(\pm 45/-45/90)_S$ stiffener web layup. This design also ensures that plies in all structural elements are oriented in at least three directions for laminate stability.

Test Specimens and Experimental Setup

A photograph of the foam-filled hat-stiffened panel is shown in Figure 3. Four such four-stiffener panels were fabricated. One of these panels was cut up to produce four 30-in.-long single-stiffener specimens for performing stiffener crippling tests with and without damage. Additional single-stiffener specimens of shorter length were fabricated using the panel trimmings to generate more damage tolerance information for this structural concept. Shorter single-stiffener specimens (6.75-in. long) were designed such that the skin buckles into three half-waves to represent the response of the 30-in.-long crippling specimens which buckles into seven half-waves. The ends of both the large panel and single-stiffener specimens were potted, and machined flat and parallel to introduce the load. Both types of single-stiffener specimens were tested as wide columns. The sides of the large panels were simply supported using knife edges to prevent the unsupported skin from buckling and prematurely initiating panel failure. The location of the strain and displacement measuring instrumentation was based on finite element analysis results for both the single-stiffener and panel specimens. The strain gage instrumentation was located at the mid length of the single-stiffener specimen on the stiffener cap, skin, and skin-stiffener flange locations. For the large panels, additional gages were placed at other locations as well. Displacement transducers were used to monitor specimen end shortening and out-of-plane displacements at appropriate pre-determined locations and shadow moiré interferometry was used to obtain a field view of the out-of-plane displacement contours.

Results and Discussion

Experimental Results

In the experimental program, two types of specimens were tested which are shown in Figure 4. The first type of specimens are single-stiffener specimens of two different lengths, one to study the response without and with barely visible impact damage due to airgun and dropped-weight impactors, and the second to study the response due to airgun impacts at higher energy levels. The second type of specimens are multi-stiffener specimens which were tested in compression without and with combinations of airgun and dropped-weight impact damage. The objective of these tests was to gain an understanding of the damage tolerance characteristics of the foam-filled hat-stiffener panel concept.

Impact Energy Levels for Barely Visible Damage Initiation

One of the 30-in.-long single-stiffener specimens was dedicated to perform impact studies to determine the threshold energy levels for damage initiation at different structural locations. The selected locations are at the skin, stiffener cap, and skin-stiffener flange interface. Dropped-weight and airgun-propelled 0.5-in.-diameter aluminum ball impactor tests were performed at increasing energy levels to determine these threshold levels. The damage initiation threshold energy levels for the skin and skin-stiffener flange interface subjected to airgun impacts from the skin side of the panel are 1.60 ft-lb (125 ft/sec) and

2.25 ft-lb (150 ft/sec), respectively. The stiffener cap of the specimens was impacted with a dropped-weight impactor to simulate impact due to dropped tools. The resulting damage initiation threshold energy level was determined to be 15 ft-lb.

Single-stiffener Specimen Tests

As the undamaged 30-in.-long specimen was loaded quasi-statically, the skin buckled at about 33,500 lb and further loading of the element specimen resulted in failure at 36,080 lb. The out-of-plane displacement contours of the specimen is shown in Figure 5(a). At the instance of failure, the skin had seven half-waves along the length of the specimen. The failure appeared to initiate along the nodal line slightly below the mid-length of the specimen due to high interlaminar stresses and then it propagated across the width of the specimen as shown in Figure 5(b). The failure is characterized by a clean break of the foam-filled stiffener.

The second 30-in.-long single-stiffener specimen was compression tested after subjecting the stiffener cap to dropped-weight impact. This test was intended to study the response of the single-stiffener specimen in the presence of impact damage due to dropped tools in a structural assembly or maintenance environment. After subjecting the stiffener cap at the mid length of the specimen to an impact at 20 ft-lb, which is 5 ft-lb more than the threshold level for damage initiation, the specimen was loaded in compression. As the loading was increased, the specimen skin buckled at approximately 33,500 lb and the final failure of the specimen occurred at 35,552 lb. The out-of-plane displacement contours of the specimen at failure and the failure mode are shown in Figures 6(a) and 6(b). The failure mode was very similar to the single-stiffener failure mode without damage. This result suggests that the imposed damage condition of 20 ft-lb on the stiffener cap does not result in any reduction in strength. The impact test with the dropped weight was limited to an energy level that is slightly above the energy level that corresponds to barely visible impact damage with the understanding that if the damage due to dropped tools on the ground is visible, the structure will be repaired or replaced.

The last 30-in.-long single-stiffener specimen was subjected to an airgun-propelled impact at the skin-stiffener flange interface. This damage was intended to simulate impact to the exterior of the structure due to runway debris and hailstones. Also, impact at this location is more critical to the specimen strength than impact to the skin. The specimen was impacted at its mid-length with 3.1 ft-lb of impact energy, 30 percent more than the damage initiation threshold, which corresponds to 16 percent higher speed for the 0.5-in.-diameter aluminum impactor. The location of impact is identified in Figure 7(a) where out-of-plane deflection contours of the specimen at failure is shown. The failed specimen is shown in Figure 7(b). Failure initiated from the impact damaged skin-stiffener flange interface location and propagated across the width of the specimen in a catastrophic manner before the skin could buckle. The specimen failed at an applied load of 31,304 lb which is 15 percent lower than the undamaged specimen failure load. The failure mode can also be seen in the figure.

The end-shortening results for the 30-in.-long single-stiffener specimens are summarized in Figure 8. In this figure, end-shortening results are normalized by the overall length of the specimen and then plotted against the total applied load normalized by the axial stiffness of the specimen. Thus, the numbers along the abscissa and the ordinate

represent global axial strains. The open circles, squares, and triangles represent data for specimens without damage, with airgun impact damage, and with dropped-weight impact damage, respectively. The solid symbols represent the corresponding failure events. All specimens exhibit nonlinear behavior beyond approximately 33,000 lb, which is the load at which skin buckling occurred. The specimens without damage and dropped-weight impact damage failed at an axial strain of 7,500 μ in/in. while the specimen with airgun impact damage at the skin-stiffener flange location failed at 6,000 μ in./in. suggesting that the latter is a more critical damage case.

The measured strain results for the undamaged 30-in.-long single-stiffener specimen are plotted in Figure 9. The strain gages are mounted across the specimen at mid-length. All strain gages except gage 2 indicate a similar global bending trend which is nonlinear beyond approximately 15,000 lb. The initial response of gage 2 suggests local bending of the skin element under the stiffener and strain reversal at about 33,000 lb indicates local buckling of the skin. The maximum value for the local strains at failure is approximately 7,500 μ in./in.

The results presented above on the 30-in.-long single-stiffener specimens demonstrate that the concept is very tolerant to impact levels that are 30 percent above the damage initiation threshold levels. To determine the response of the panel subjected to impacts at higher energy levels, several specimens of smaller length were tested. The response of these specimens, which are shorter than the 30-in.-long single-stiffener specimen that deformed into seven halfwaves at the time of failure, is expected to exhibit behavior that could be directly compared.

Out of the five 6.75-in.-long single-stiffener specimens that were available, one was tested without damage to provide reference data and the rest were tested with airgun impact damage to either the skin opposite to the stiffener or with damage at the skin-stiffener flange interface along the mid-length of the specimen. The undamaged specimen buckled into three half-waves at approximately 22,000 lb axial load and failed at 39,800 lb. The next two specimens were impacted with airgun impact energy levels of 3.06 ft-lb (175 ft/sec) and 12.75 ft-lb (357 ft/sec) on the skin opposite to the stiffener. The damaged regions of these specimens could not be distinguished from the C-scans due to the presence of foam core opposite to the point of impact on the skin. When loaded, the specimens buckled at approximately 20,000 lb and damage in both these specimens grew as evidenced by the moiré fringes shown in Figure 10. The final failure of these specimens occurred at 27,477 and 27,290 lb, respectively, which is approximately 31 percent below the undamaged specimen failure load.

The remaining two 6.75-in.-long specimens were damaged at a skin-stiffener interface location along the mid-length of the specimen with airgun impact energy levels of 3.27 ft-lb (179 ft/sec) and 12.25 ft-lb (350 ft/sec), respectively. The extensive nature of the damaged regions for these specimens was noticed by scanning the damaged area with a hand-held probe. When the specimen impacted at an impact energy level of 3.27 ft-lb was loaded, the panel buckled at approximately 23,000 lb with no growth in the damage until it failed at 36,372 lb, which is only 8.5 percent lower than the undamaged specimen failure load. The compression response of this specimen is shown in Figure 11. For the 12.25 ft-lb impact energy case, specimen buckling did not occur and the damage grew as shown in Figure 12 before final failure occurred at 22,354 lb. A reduction in load carrying capability

of 44 percent resulted for this damage case which is the maximum load-reduction value for all the single-stiffener cases investigated in this paper.

Multi-stiffener Panel Specimen Compression Tests

The multi-stiffener panels were tested with the long edges simply supported. As the undamaged panel was loaded, it exhibited observable out-of-plane displacement at approximately 50,000 lb in the form of two lobes that were positioned to the left and right of the centerline of the test specimen as shown in Figure 13. As the loading was increased, the skin in the central bay of the specimen buckled at approximately 125,000 lb with further loading resulting in failure of the specimen at 133,828 lb. The out-of-plane displacement contour at failure is shown on the left of the figure. The failure appears to have originated along the skin buckle nodal line below the mid-length of the specimen. The failure propagated catastrophically following the nodal line direction to the boundaries. The failure surface of the specimen is shown on the right of the figure.

The second multi-stiffener panel was subjected to airgun impact damage at three locations on the skin side of the panel to assess the criticality of the damage location on the residual strength and failure mode. A 0.5-in.-diameter aluminum ball was used to impact the specimen with a speed of 175 ft/sec at the skin-stiffener flange interface location and with a speed of 150 ft/sec at two skin locations. One skin location was in the mid-bay of the panel approximately 8 inches below the upper potted end and the other location was in the side bay approximately 8 inches above the lower potted end. The locations of the impact damage are shown in Figure 14. The skin impact in the mid-bay is considered more critical due to the skin local buckling in this region that precedes failure. As the specimen was loaded, failure initiated at the skin-stiffener flange interface location before skin buckling could occur and damage propagated catastrophically across the width of the panel. The failure surface is shown on the right of the figure. The failure load was 118,470 lb which is 13 percent lower than the failure load of the undamaged panel specimen.

The third multi-stiffener panel was subjected to a combination of airgun and dropped-weight impact damage and loaded to failure in this experiment. The airgun impact speed was 150 ft/sec at the same two skin locations described for the previous test and the dropped-weight impact was on the stiffener cap. The stiffener to the left of the center line shown in Figure 15 was impacted first at a 15 ft-lb energy level and then the specimen was loaded to 2/3 of the undamaged failure load for the panel. The panel specimen was then unloaded and the stiffener to the right of the center line of the panel was impacted at a 20 ft-lb energy level before reloading it to failure. When loaded, failure initiated at the skin impact location in the mid-bay and propagated across the width of the specimen. The failure load corresponding to this failure was 118,887 lb. Considering that the element specimen subjected to a 20 ft-lb dropped-weight impact energy level had no degradation in behavior, it appears that damage to the skin is the more critical damage for this foam-filled stiffener concept.

The end-shortening results for all the multi-stiffener panels are summarized in Figure 16. The out-of-plane displacement results normalized by the length of the specimen are plotted as a function of the total applied load normalized by the axial stiffness. The response for all the panel specimens tested is nonlinear. The damaged panels exhibit a 13 percent degradation in load carrying ability compared to the undamaged panel specimen

results. The response of the panel subjected to a 20 ft-lb dropped-weight impact retraces the response of the panel subjected to a 15 ft-lb impact suggesting that the 20 ft-lb impact did not result in a stiffness degradation. The global strain at failure is approximately 5,500 μ in./in. for the panels.

The strain results in the skin at mid-length for all the panel test specimens are presented in Figure 17. The specimen response was consistent in all tests. In the case of the undamaged panel, the skin buckled at approximately 125,000 lb as indicated by the strain reversal in one of the back-to-back gages. The out-of-plane displacement contours from moiré interferometry confirmed local skin buckling in the mid-bay of the panel at this load value. The strain levels in the skin of the damaged specimens corresponding to the failure event are approximately 7,000 μ in./in.

Analytical Results

Finite element analysis of the single- and multi-stiffener specimens was performed to correlate the undamaged specimen behavior. The DIAL finite element code (Ref. 4) was used to perform buckling and nonlinear static analyses. The finite element models were generated using shear deformable plate elements. Linear static and bifurcation buckling analyses were performed prior to testing the specimens to help make instrumentation and loading decisions. The geometrically nonlinear analyses were performed after the test to correlate the displacement and strain levels. Nonlinear analysis results are obtained by using the Newton-Raphson method.

The experimental end-shortening results for the single-stiffener specimen are compared with analytical results in Figure 18. The analysis results are represented by the solid line and the experimental results are represented by the open circles. The filled circle indicates the failure event. The correlation between the results is good. The single-stiffener specimen buckling response is compared with the finite element analysis results in Figure 19. From moiré interferometry results and strain gage readings it appears that the element specimen skin buckled into six half-waves at approximately 33,625 lb. The analysis predicts this first buckling mode to occur at 34,502 lb with the same number of half-waves.

The experimental and analytical end-shortening results for the multi-stiffener specimens are presented in Figure 20. The analytical results are represented by a solid line and the experimental results are represented by open squares. The filled square represents the failure event for the specimen. The nonlinear response compares well with the analytical results. The panel static response is compared with the experimental results in Figure 21. As discussed earlier, the panel exhibited observable out-of-plane deformations for loads greater than 50,000 lb in the form of two lobes at the central stiffener locations. The nonlinear analysis results are compared with the experimental results in this figure for a load of 75,000 lb. The comparison between the analytical and experimental out-of-plane displacement contour is good.

Concluding Remarks

Design, analytical, and experimental studies have been conducted to evaluate a foam-filled hat-stiffened panel concept. Design studies suggest that using this new concept

could result in 6 to 10 percent improvement in structural efficiency compared to a more conventional hat-stiffened panel. The foam-filled hat-stiffened concept is amenable to automated manufacturing processes that are suitable for solid-blade-stiffener geodesic structures and are 20 percent lighter than the solid-blade-stiffener panels in the 3,000 to 20,000 lb/in. axial load range.

Single and multi-stiffener specimen test results indicate that 20 ft-lb dropped-weight impact damage to the stiffener cap does not result in significant degradation of performance. Multi-stiffener panel and single-stiffener test results suggest that airgun impact damage to the skin at the skin-stiffener flange interface at an impact energy level of 3.10 ft-lb, which is 30 percent more than the energy level for barely visible impact damage, results in a reduction of approximately 12 percent in the load carrying capability. The single-stiffener test results indicate that a 3.10 ft-lb airgun impact to the skin opposite to the stiffener cap can result in a degradation of the failure load by about 30 percent. An increase in the impact energy level to 12.25 ft-lb at the same location for the single-stiffener specimen resulted in a similar degradation in load carrying capability. This result suggests that the skin and foam core interface might have been damaged locally at or above impact energy levels of 3.10 ft-lb. An airgun impact at 12.75 ft-lb to the skin at the skin-stiffener flange interface resulted in a maximum degradation of 44 percent in load carrying capacity for the single-stiffener specimen. The critical locations for impact damage are the skin opposite to the stiffener cap and the skin-stiffener interface. The global failure strain was greater than 5,500 μ in./in. for all test specimens with and without impact damage. The analytical results for buckling and postbuckling responses compare well with the experimental results.

References

1. Reddy, A. D., Rehfield, L. W., Haag, R. S., and Wideman, C. B.: Compressive Buckling Behavior of Graphite/Epoxy Isogrid Wide Columns with Progressive Damage. Compression Testing of Homogeneous Materials and Composites, ASTM STP 808, edited by R. Chair and R. Paperino, 1983, pp. 187-199.

2. Ambur, D. R., and Rehfield, L. W.: Effect of Stiffness Characteristics on the Response of Composite Grid-stiffened Structures. Journal of Aircraft, Vol. 30, No. 4, July-August 1993, pp. 541-546.

3. Stroud, W. J., and Anderson, M. S.: PASCO: Structural Panel Analysis and Sizing Code, Capability and Analytical Foundations. NASA TM-80181, November 1981.

4. Anon.: DIAL Finite Element Analysis System - Version L3D2. Lockheed Missiles and Space Company, July 1987.

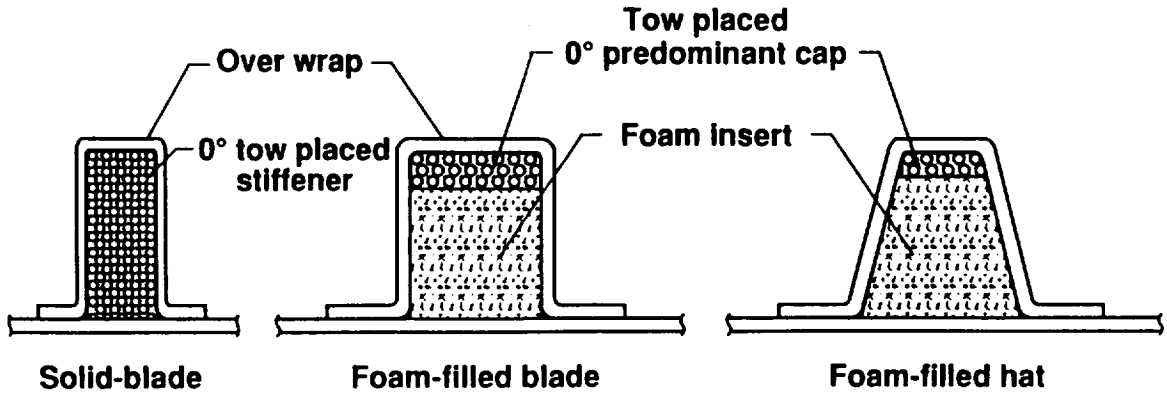

Figure 1. Foam-filled stiffener concepts.

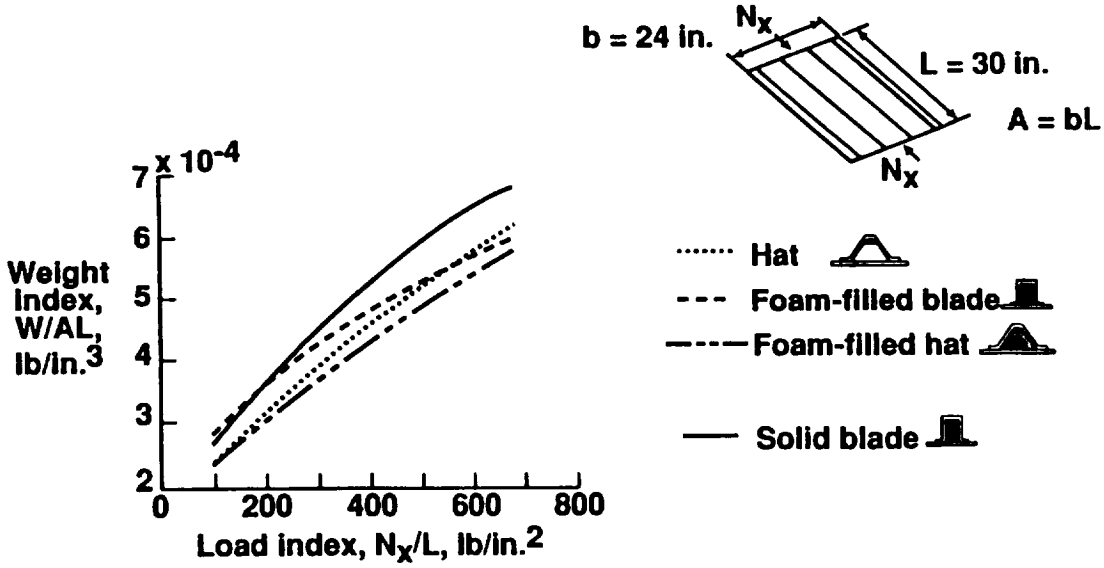

Figure 2. Structural efficiency of foam-filled stiffener panel concepts.

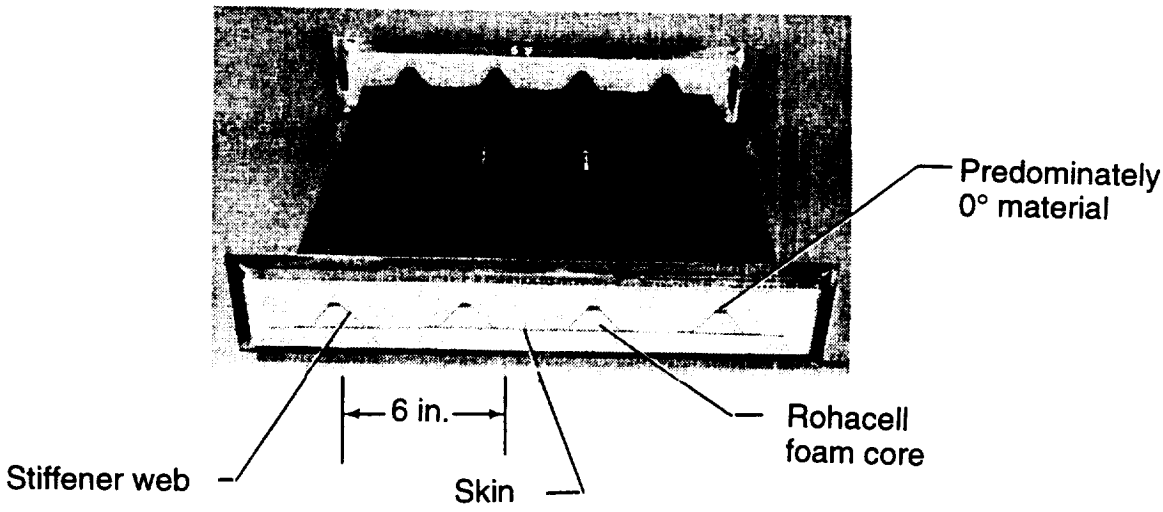

Figure 3. Foam-filled hat-stiffened panel.

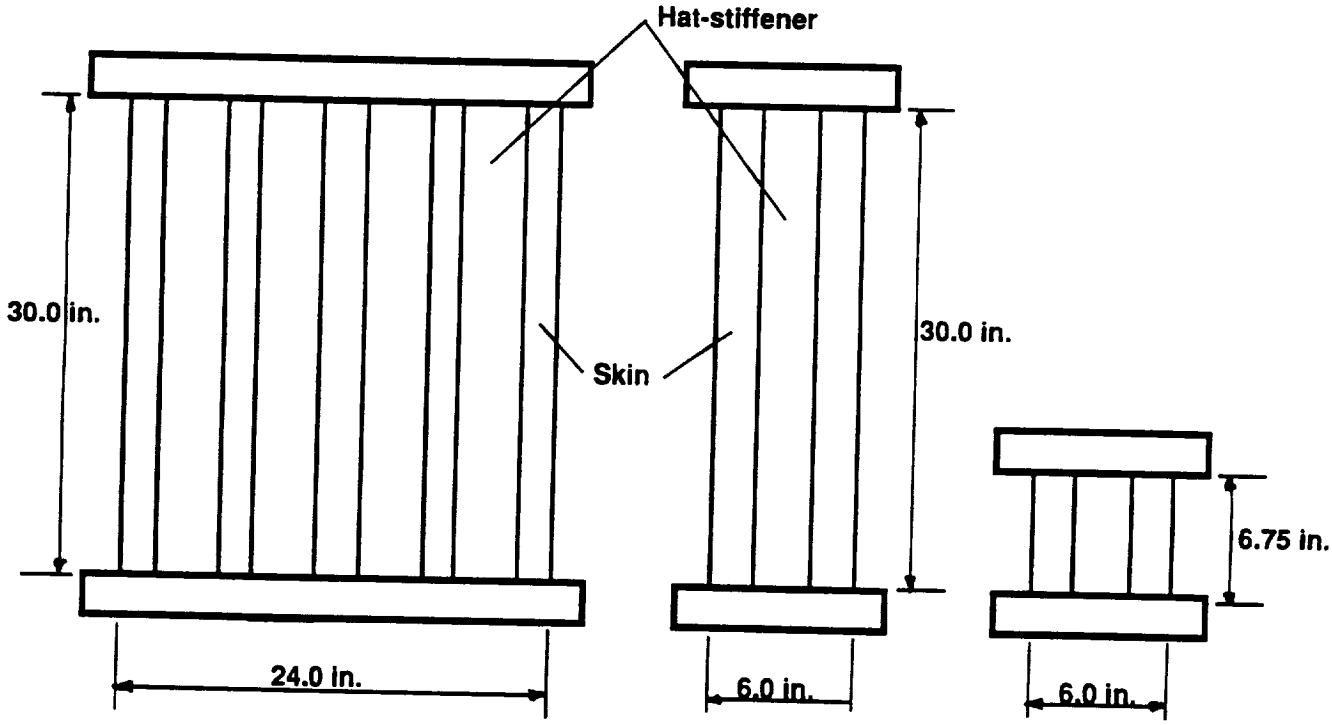

Figure 4. Types of test specimens.

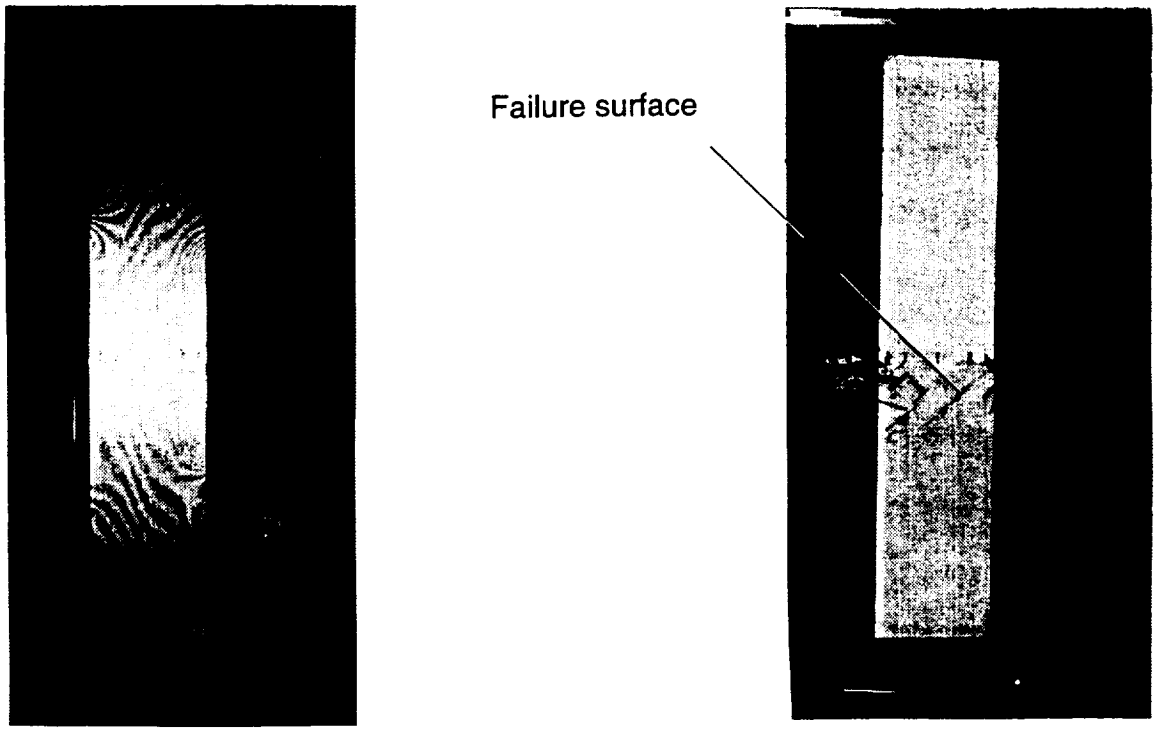

(a) Out-of-plane deflection contour (b) Failure mode

Figure 5. Failure mode of an undamaged 30-in. long single-stiffener specimen.

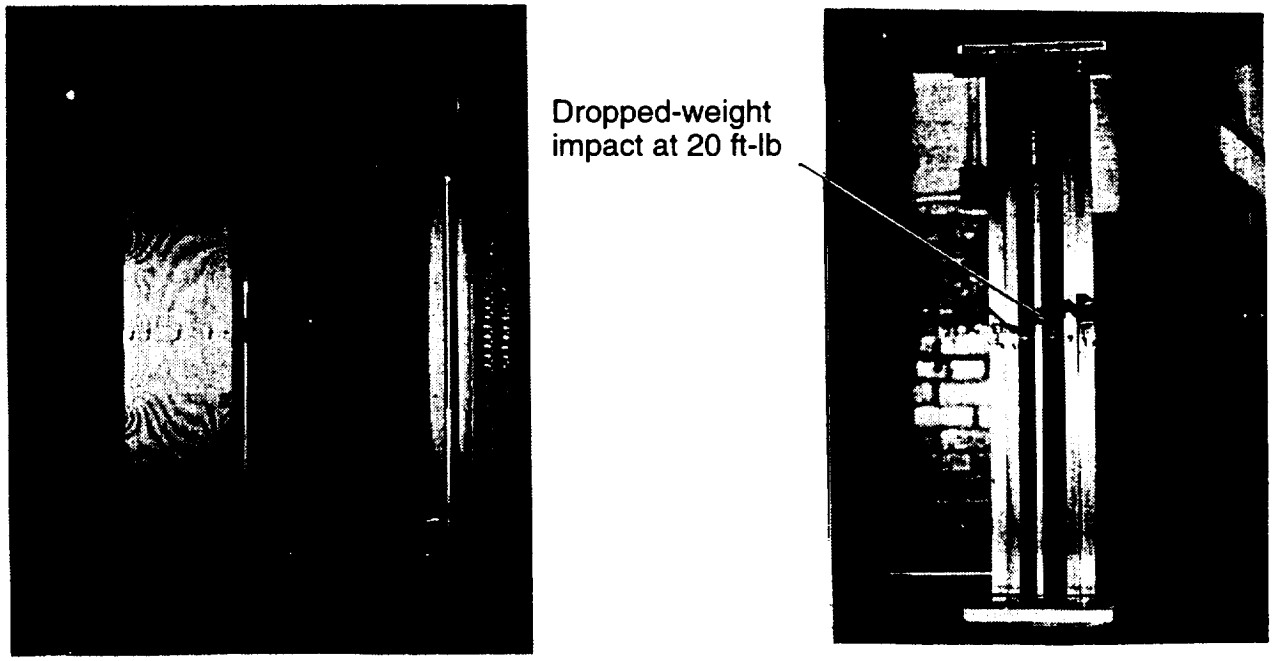

(a) Out-of-plane deflection contour (b) Failure mode

Figure 6. Failure mode of 30-in. long single-stiffener specimen subjected to dropped-weight impact.

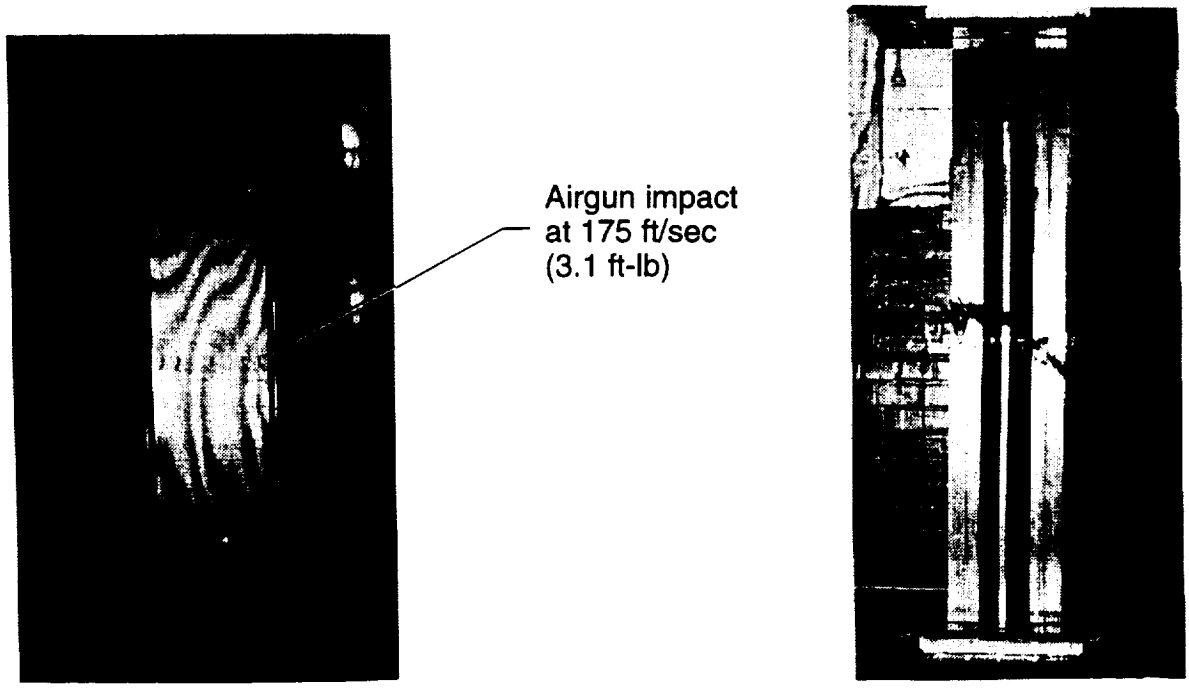

(a) Out-of-plane deflection contour (b) Failure mode

Figure 7. Failure mode of a 30-in. long single-stiffener specimen subjected to an airgun impact.

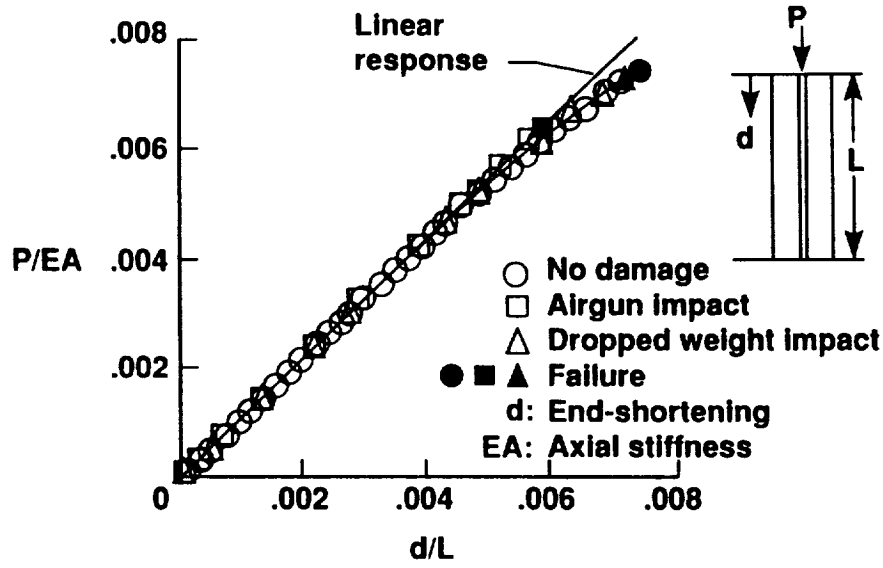

Figure 8. Summary of load versus end-shortening results for 30-in. long single-stiffener specimens.

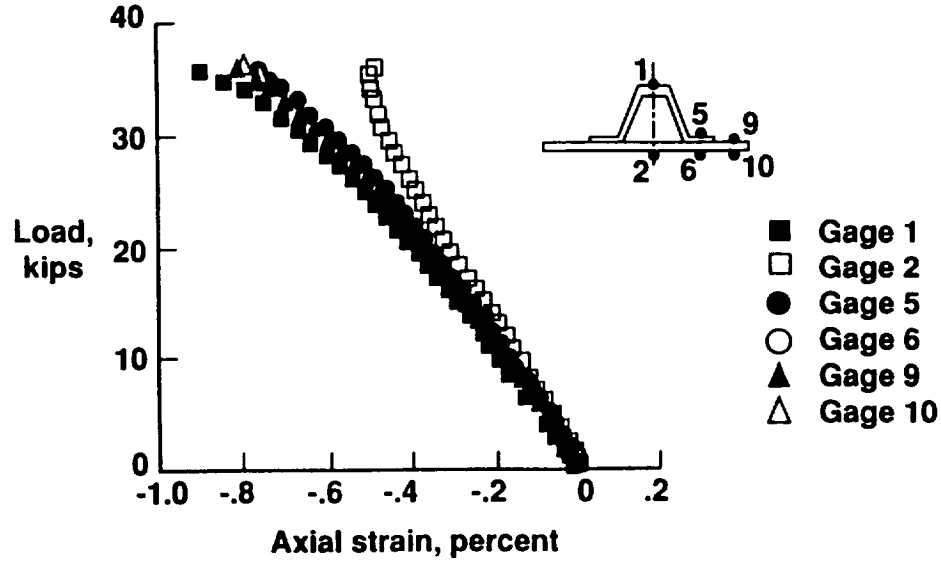

Figure 9. Typical axial strain results for an undamaged 30-in.-long single-stiffener specimen.

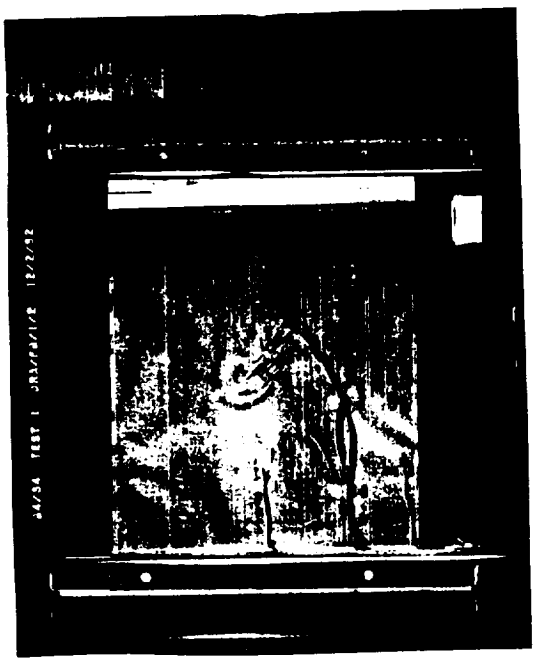

(a) Out-of-plane displacement contour - 3.06 ft-lb impact case

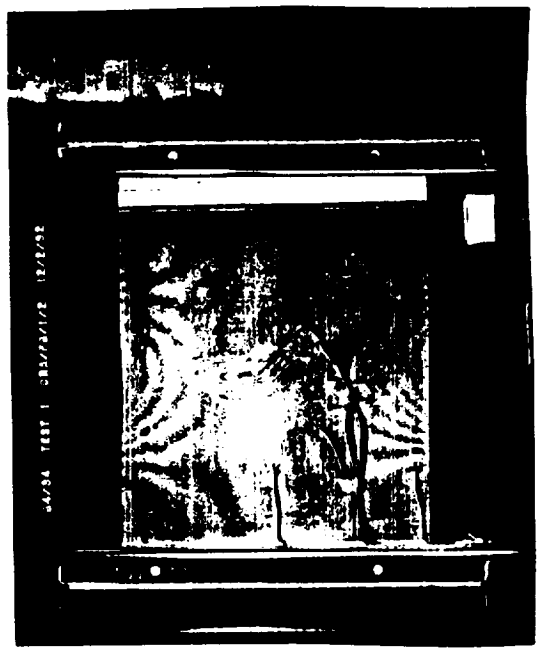

(b) Out-of-plane displacement contour - 12.75 ft-lb impact case

Figure 10. Compression response of 6.75-in.-long single-stiffener specimens subjected to airgun impact at skin location opposite to the hat-stiffener cap.

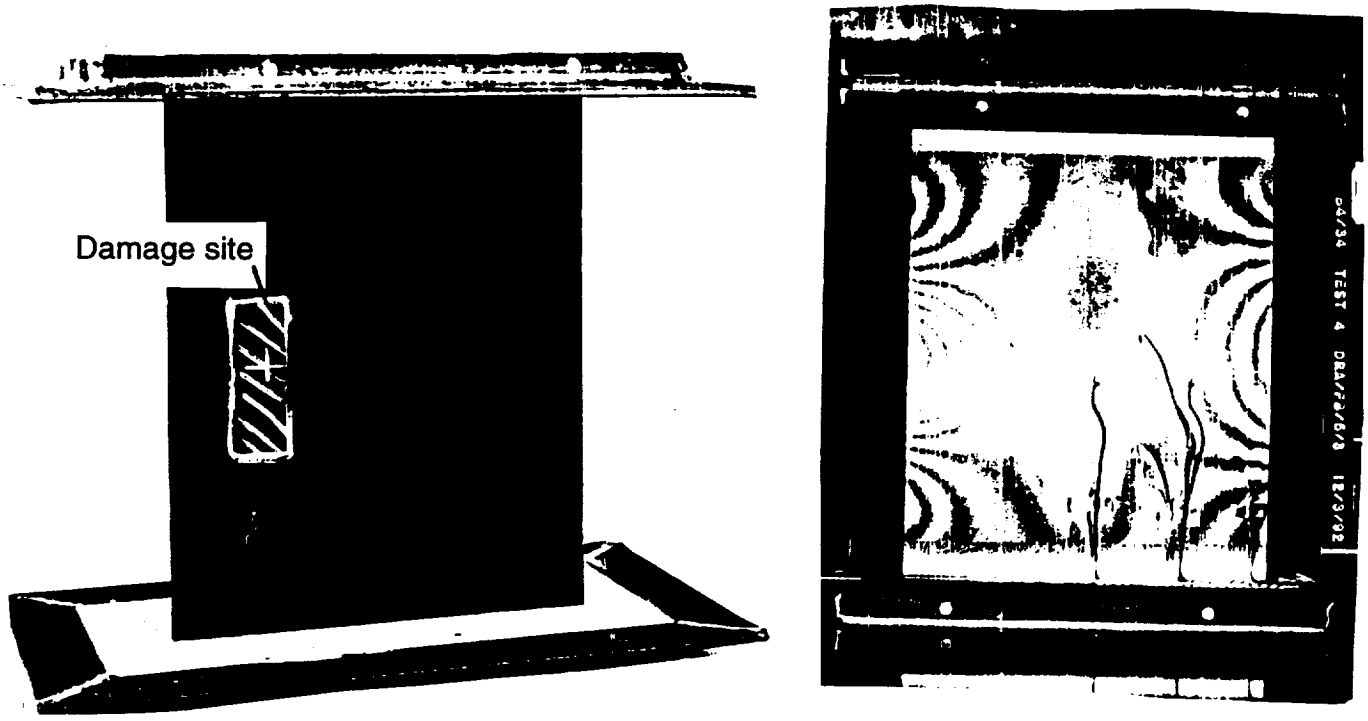

(a) Damage location and size

(b) Out-of-plane displacement contour

Figure 11. Compression response of a 6.75-in.-long single-stiffener specimen subjected to 3.27 ft-lb airgun impact at skin location opposite to the skin-stiffener flange interface.

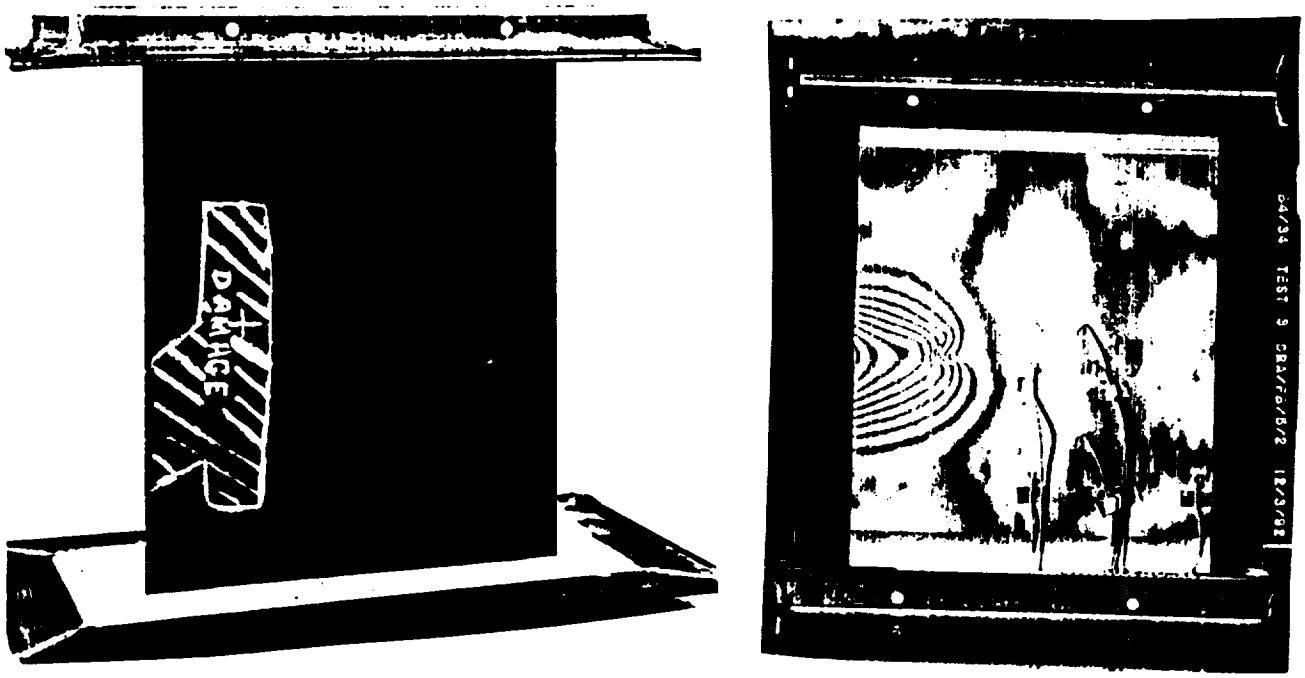

(a) Damage location and size

(b) Out-of-plane displacement contour

Figure 12. Compression response of a 6.75-in.-long single-stiffener specimen subjected to 12.25 ft-lb airgun impact at skin location opposite to the skin-stiffener flange interface.

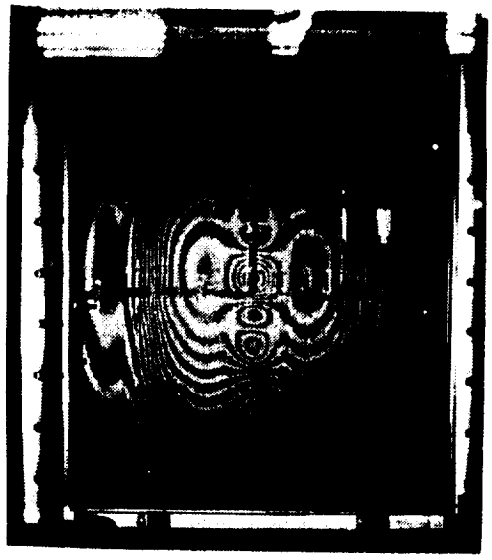

Out-of-plane displacement
Contour at failure

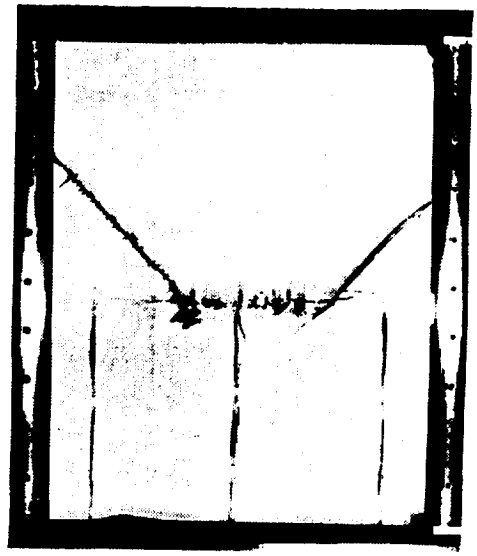

Failure mode
Skin side

Figure 13. Failure mode of an undamaged multi-stiffener panel specimen.

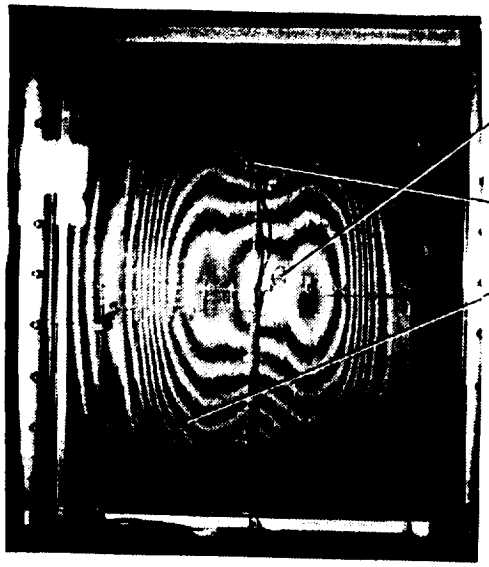

Out-of-plane deflection
Contour at failure

Failure mode
Stiffener side

Figure 14. Failure mode of a multi-stiffener panel specimen subjected to an airgun impact.

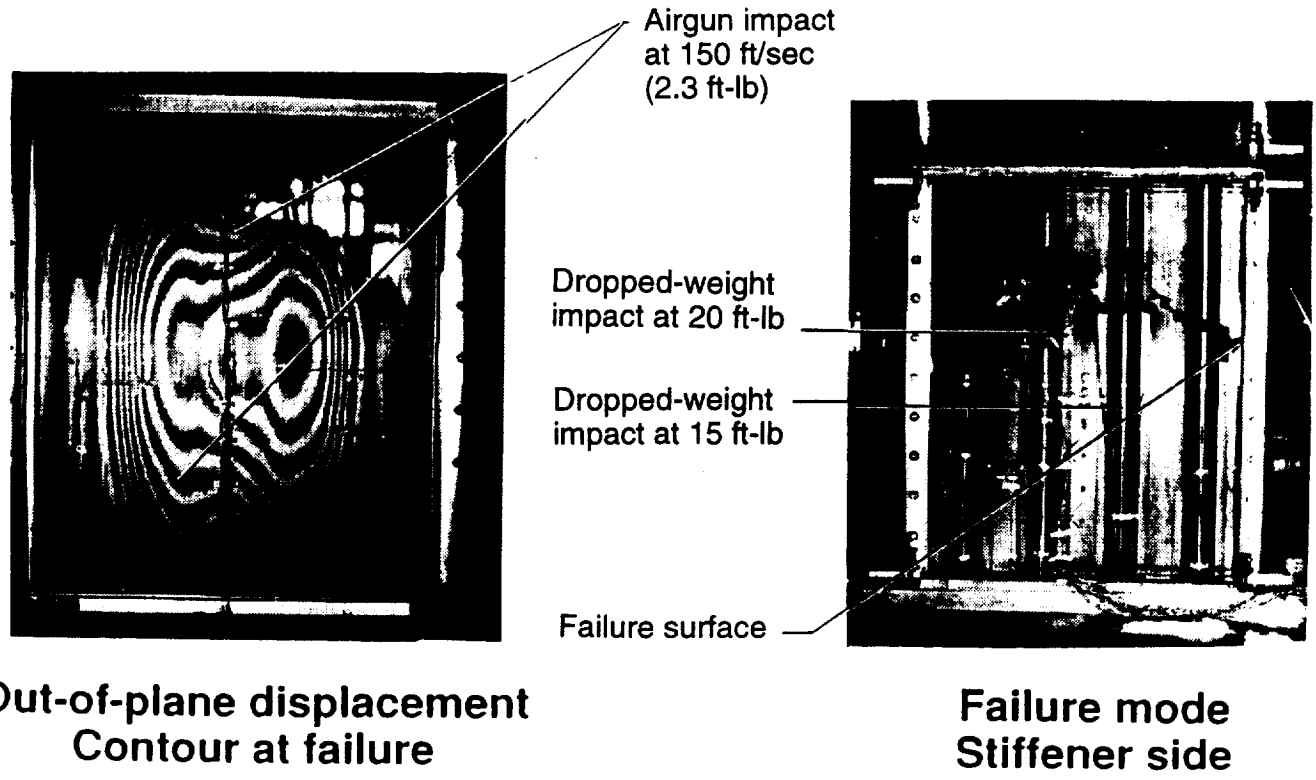

Figure 15. Failure mode of a multi-stiffener panel specimen subjected to airgun and dropped-weight impacts.

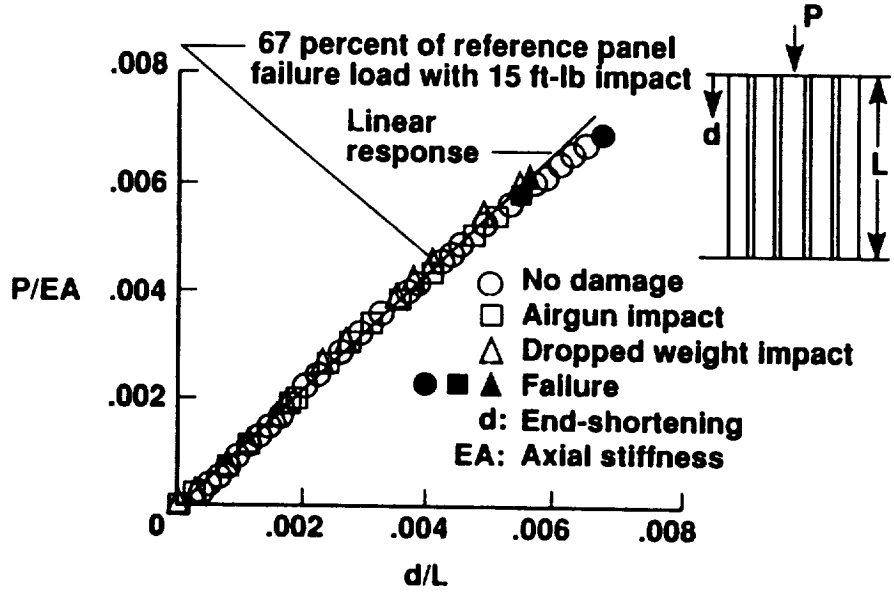

Figure 16. Summary of load versus end-shortening results for multi-stiffener panel specimens.

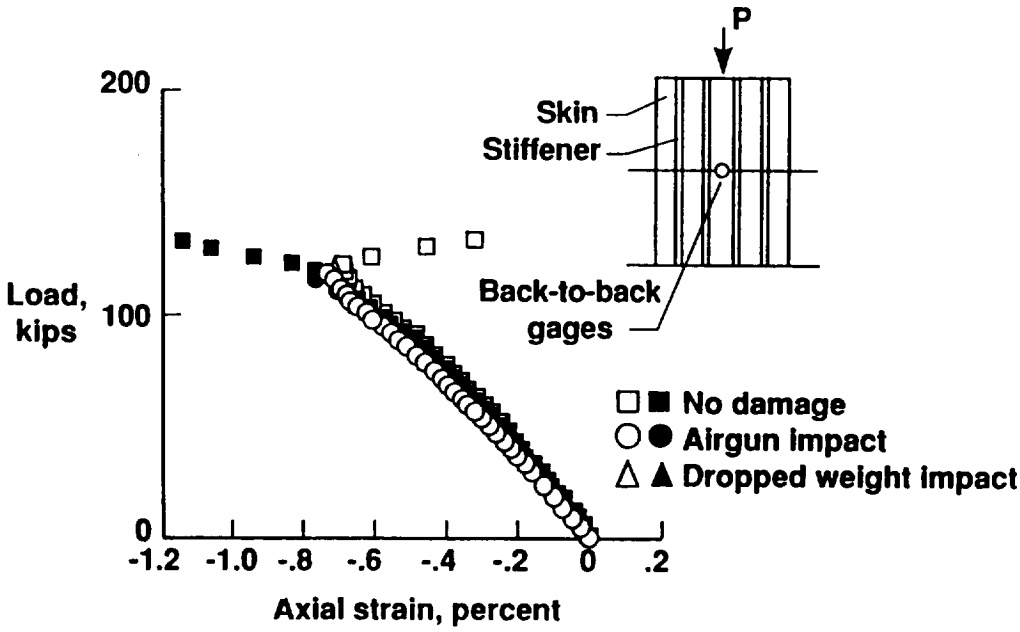

Figure 17. Strain results for multi-stiffener panel specimens at a skin location.

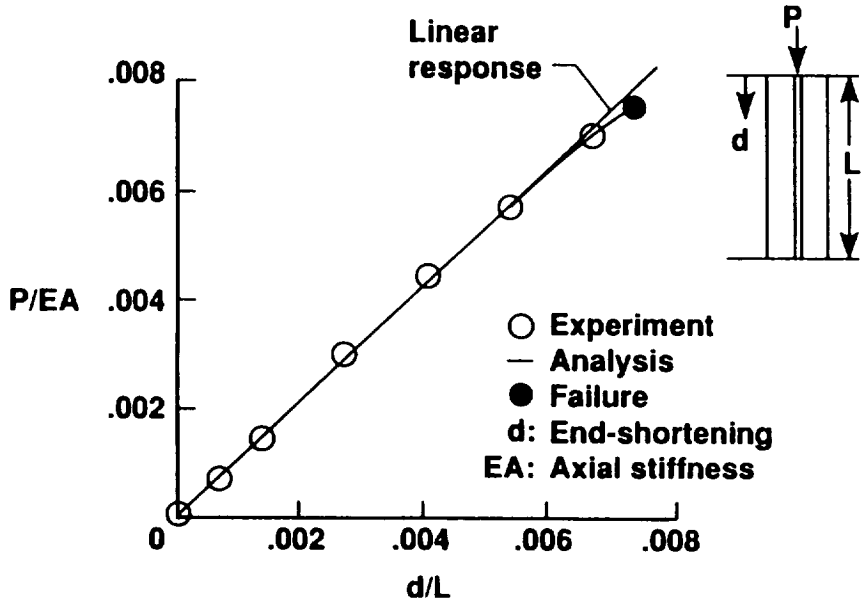

Figure 18. Correlation of experimental and analytical end-shortening results for an undamaged 30-in.-long single-stiffener specimen.

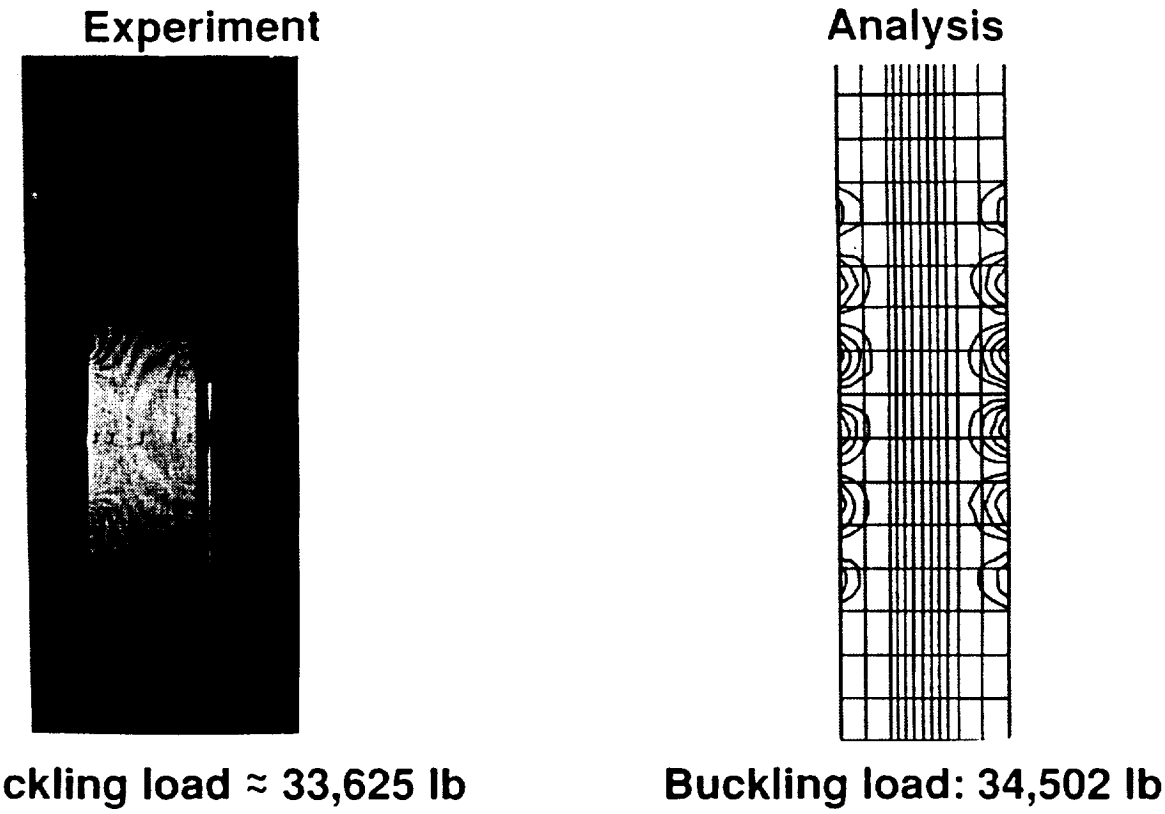

Figure 19. Comparison of experimental and analytical buckling response for an undamaged 30-in.-long single-stiffener specimen.

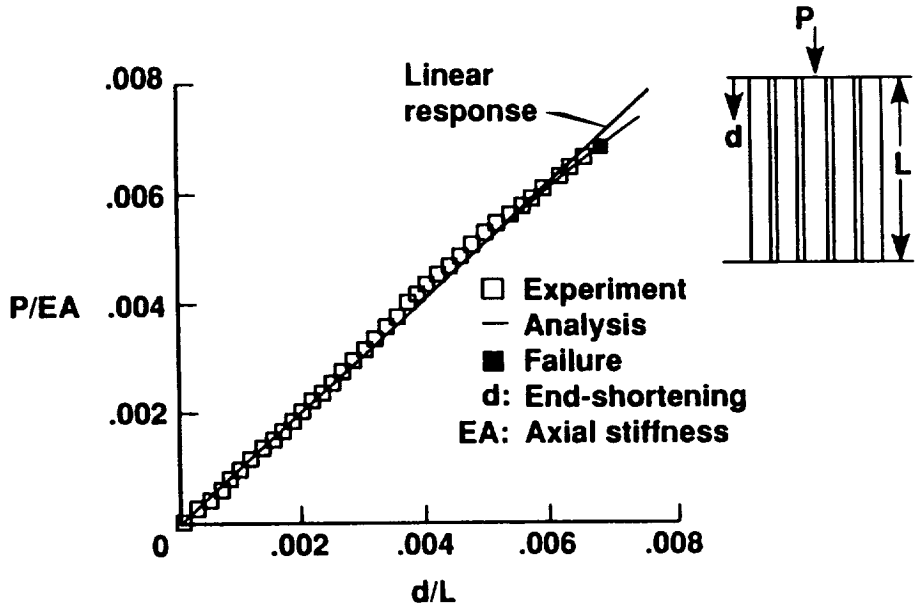

Figure 20. Correlation of experimental and analytical end-shortening results for an undamaged multi-stiffener panel specimen.

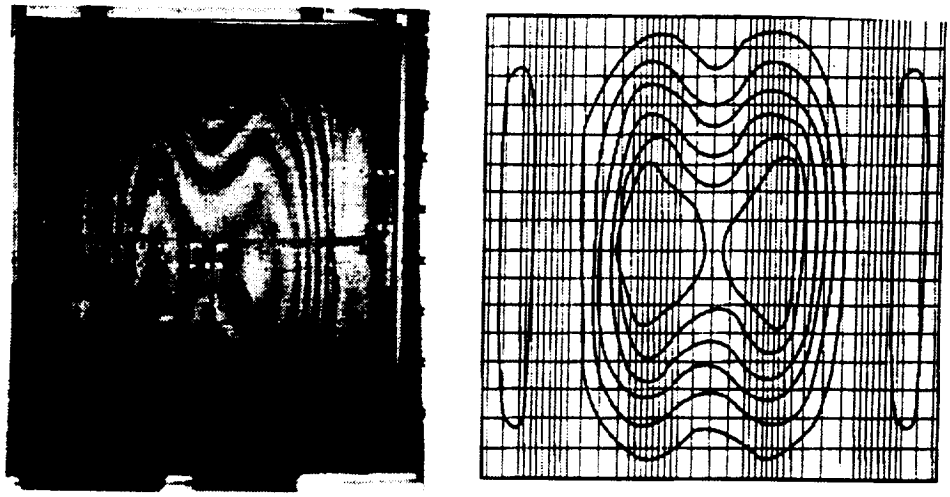

a. Experiment

b. Analysis

Figure 21. Comparison of experimental and analytical out-of-plane displacement contours for an undamaged multi-stiffener panel specimen with an applied load of 75,000 lb.

REPORT DOCUMENTATION PAGE

Form Approved
OMB No. 0704-0188

1. AGENCY USE ONLY (*Leave blank*)	2. REPORT DATE	3. REPORT TYPE AND DATES COVERED
	January 1995	Technical Memorandum

4. TITLE AND SUBTITLE
Design and Evaluation of a Foam-Filled Hat-Stiffened Panel Concept for Aircraft Primary Structural Applications

5. FUNDING NUMBERS
WU 505-63-50-08

6. AUTHOR(S)
Damodar R. Ambur

7. PERFORMING ORGANIZATION NAME(S) AND ADDRESS(ES)
NASA Langley Research Center
Hampton, VA 23681-0001

8. PERFORMING ORGANIZATION REPORT NUMBER

9. SPONSORING / MONITORING AGENCY NAME(S) AND ADDRESS(ES)
National Aeronautics and Space Administration
Washington, DC 20546-0001

10. SPONSORING / MONITORING AGENCY REPORT NUMBER
NASA TM 109175

11. SUPPLEMENTARY NOTES
Paper presented at the Third Advanced Composites Technology Conference in June 1992.

12a. DISTRIBUTION / AVAILABILITY STATEMENT
Unclassified-Unlimited
Subject Category-24

12b. DISTRIBUTION CODE

13. ABSTRACT (*Maximum 200 words*)

A structurally efficient hat-stiffened panel concept that utilizes a structual foam as stiffener core has been designed for aircraft primary structural applications. This stiffener concept utilizes a manufacturing process that can be adapted readily to grid-stiffened structural configurations which possess inherent damage tolerance characteristics due to their multiplicity of load paths. The foam-filled hat-stiffener concept in a prismatically stiffened panel configuration is more efficient than most other stiffened panel configurations in a load range that is typical for both fuselage and wing structures. The prismatically stiffened panel concept investigated here has been designed using AS4/3502 preimpregnated tape and Rohacell foam core and evaluated for its buckling and postbuckling behavior with and without low-speed impact damage. The results from single-stiffener and multi-stiffener specimens suggest that this structural concept responds to loading as anticipated and has good damage tolerance characteristics.

14. SUBJECT TERMS		15. NUMBER OF PAGES
composites structural concepts buckling	damage tolerance geodesic	20
		16. PRICE CODE A03

17. SECURITY CLASSIFICATION OF REPORT	18. SECURITY CLASSIFICATION OF THIS PAGE	19. SECURITY CLASSIFICATION OF ABSTRACT	20. LIMITATION OF ABSTRACT
Unclassified	Unclassified	Unclassified	Unlimited